

SCIENTIFIC REPORTS

OPEN

Break the Interacting Bridge between Eu^{3+} Ions in the 3D Network Structure of CdMoO_4 : Eu^{3+} Bright Red Emission Phosphor

Weiguang Ran¹, Hyeon Mi Noh¹, Sung Heum Park¹, Byung Kee Moon¹, Jung Hyun Jeong¹, Jung Hwan Kim² & Jinsheng Shi³

Eu^{3+} doped CdMoO_4 super red emission phosphors with charge compensation were prepared by the traditional high temperature solid-state reaction method in air atmosphere. The interrelationships between photoluminescence properties and crystalline environments were investigated in detail. The 3D network structure which composed by CdO_8 and MoO_4 polyhedra can collect and efficiently transmit energy to Eu^{3+} luminescent centers. The relative distance between Eu^{3+} ions decreased and energy interaction increased sharply with the appearance of interstitial occupation of O^{2-} ions (O''). Therefore, fluorescence quenching occurs at the low concentration of Eu^{3+} ions in the 3D network structure. Fortunately, the charge compensator will reduce the concentration of O'' , which can break the energetic interaction between Eu^{3+} ions. The mechanism of different charge compensators has been studied in detail. The strong excitation band situated at ultraviolet and near-ultraviolet region makes it a potential red phosphor candidate for n-UV based LED.

White light-emitting diodes (WLEDs), as the promising next generation of illumination sources to replace conventional incandescent and fluorescent lamps, have attracted much attention due to their high efficiency, long lifetime and environment-friendly characteristics^{1,2}. Phosphor-converted light-emitting diode (pc-LED) is the mainstream technology to produce solid-state illumination devices^{3,4}. Nowadays, the commercial and excellent approach is the combination of cerium-doped yttrium aluminum garnet ($\text{YAG}:\text{Ce}^{3+}$) phosphor and blue InGaN LED chip which was first proposed in 1997⁵. However, there are some disadvantages owing to the innate deficiency of this design such as poor color rendering ability, low chromatic stability under different driving currents, low efficiency and low color rendering index^{6,7}. Therefore, white LEDs which fabricated by near-UV LED chips and tri-color phosphors might conquer the aforementioned pitfalls^{2,8}. Meanwhile, with the development of LED chip technology, the emission bands of LED chips shifted from blue light to near-UV range which can offer higher energy to pump the phosphor⁹. For the above reasons, more and more attentions have been paid on phosphors with high absorption in the near-UV spectral region¹⁰⁻¹².

Cadmium molybdate CdMoO_4 with scheelite-type structure have attracted considerable interest due to its potential applications in phosphors, scintillators, magnets and catalysts^{13,14}. Eu^{3+} -doped metal molybdates is a kind of potential red emitting phosphor due to their predominant ${}^5\text{D}_0 \rightarrow {}^7\text{F}_2$ transition emission, whereas the other emissions are very weak¹⁵. It is reported that $\text{CdMoO}_4:\text{Eu}^{3+}$ shows not only desirable absorption in the near-UV region, but also excellent thermal and chemical stability¹⁶⁻¹⁸.

However, to the best of our knowledge, there are only a few reports on $\text{CdMoO}_4:\text{Eu}^{3+}$ phosphors, whether on its synthesis process or properties. For example, the optimum doping concentration of Eu^{3+} in $\text{Cd}_{1-x}\text{Eu}_x\text{MoO}_4$ phosphor prepared through microwave assisted synthesis is 5%¹⁹. Wang¹⁶ has prepared an intense $\text{CdMoO}_4:\text{Eu}^{3+}$ red emission phosphor through a facile aqueous solution route at room temperature. Guzik¹⁸ has prepared scheelite-type $\text{Cd}_{1-3x}\text{Eu}_{2x}\text{Mo}_x\text{O}_4$ phosphors by high temperature solid phase reaction method with CdMoO_4

¹Department of Physics, Pukyong National University, Busan, 608-737, South Korea. ²Department of Physics, Donggeui University, Busan, 614-714, South Korea. ³Department of Chemistry and Pharmaceutical Science, Qingdao Agricultural University, Qingdao, 266109, People's Republic of China. Correspondence and requests for materials should be addressed to J.H.J. (email: jhjeong@pknu.ac.kr)

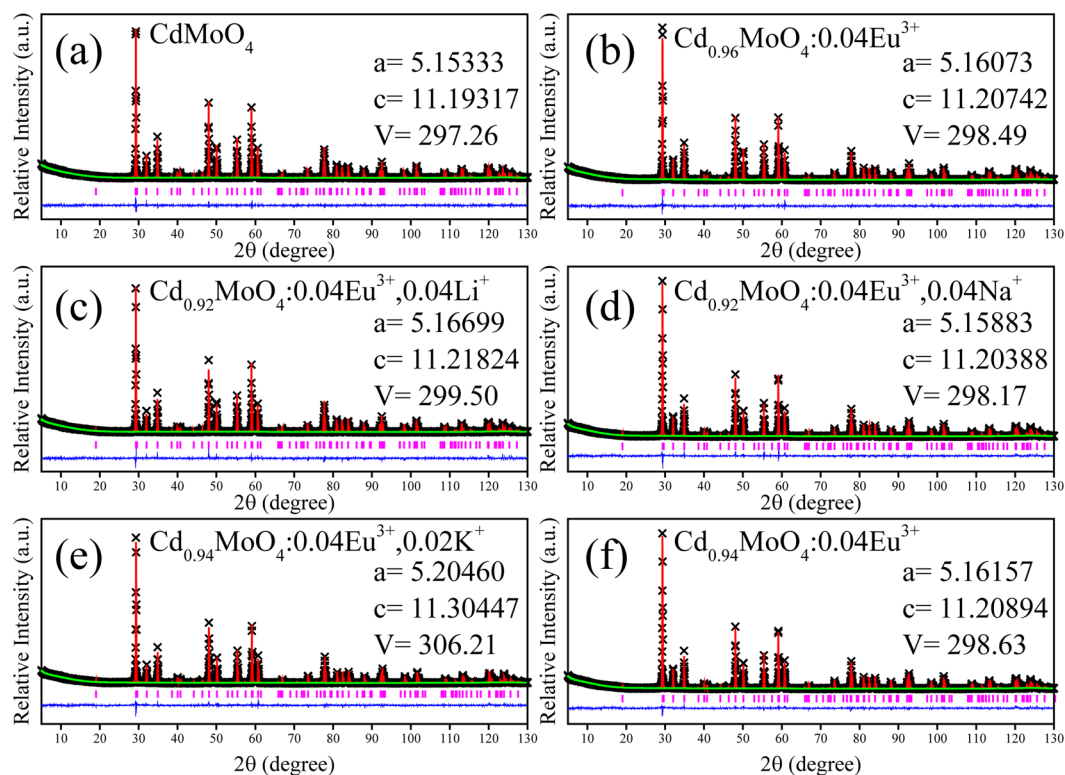


Figure 1. Final Rietveld refinement profiles of CdMoO₄, Cd_{0.96}MoO₄:0.04Eu³⁺, Cd_{0.96-y}MoO₄:0.04Eu³⁺, yM (M = Li⁺, Na⁺, K⁺ ions and Cd²⁺ vacancy) phosphors.

and Eu₂(MoO₄)₃ as start materials. And the effect of Cd²⁺ vacancy on the occupied position of doping ions in CdMoO₄ was investigated for the first time^{18,20}.

In this paper, a series of Cd_{1-x-y}MoO₄:xEu³⁺, yM (M = Li⁺, Na⁺, K⁺ ions and Cd²⁺ vacancy) phosphors have been prepared via a high temperature solid-state reaction process and their structural and photoluminescence properties were thoroughly investigated. The geometry optimization and electronic structure calculations were performed using the Cambridge Serial Total Energy Package (CASTEP) code²¹. The relationship between the photoluminescence properties and lattice environments of the doped Eu³⁺ ions with different charge compensators was discussed in detail. As the phosphor was pumped by near UV light, superior color purity and high red emission intensity with chromaticity coordinates (0.6451, 0.3451) was achieved. The charge compensation model in this 3D network structure was expected to be used to design efficient luminescent materials.

Results

Crystal Structures, Phase Identification and Purity. The structure refinement of the CdMoO₄, Cd_{0.96}MoO₄:0.04Eu³⁺ and Cd_{0.96-y}MoO₄:0.04Eu³⁺, yM (M = Li⁺, Na⁺, K⁺ and Cd²⁺ vacancy) samples was performed using the GSAS II software package²² and the initial parameters of refinement for CdMoO₄ sample were referred from the single crystal data of CdMoO₄ (ICSD-84455). All atomic positions, fraction factors and temperature factors were refined convergence and well satisfied the reflection condition. The final refinement patterns are illustrated in Fig. 1. It can be seen from Fig. 1 that the incorporation of Eu³⁺ and charge compensators affect the unit cell parameters. Cell volumes were increased with the introduction of Eu³⁺ ions. This lattice distortion occurred due to the differences of ionic radius and valence states. It appears from Fig. 1 that the unit cell parameters were effectively regulated with different charge compensators. And the introduction of Na⁺ ions can minimize the lattice distortion.

The structure model of CdMoO₄ with a 4 × 4 × 4 supercell along *a*-direction (same with *b*-direction) was shown in Fig. 2(a). Green cross chains were interconnected to form a 3D network structure. From Fig. 2(b), each CdO₈ dodecahedron connects with eight MoO₄ tetrahedra units by common vertex connection. It can be seen from Fig. 2(c) that one CdO₈ is surrounded by four CdO₈ dodecahedrons and become a tetrahedral structure by sharing common edge between each other. The three-dimensional framework in CdMoO₄ was composed of CdO₈ dodecahedron and MoO₄ tetrahedron. All of CdO₈ and MoO₄ polyhedra are connected to form a 3D network structure while MoO₄ fill in the interspace. From Fig. 2d and e, the coordination environment of Mo⁶⁺ and Cd²⁺ ions is intuitively displayed. Four coordinated Mo sites have the same Mo-O distance even eight Cd-O bonds lengths are approximate.

First-principles Calculation and Band Structures. The light absorption capability of the as prepared samples of CdMoO₄, Cd_{0.96}MoO₄:0.04Eu³⁺ and Cd_{0.92}MoO₄:0.04Eu³⁺, 0.04 Na⁺ have been evaluated using the

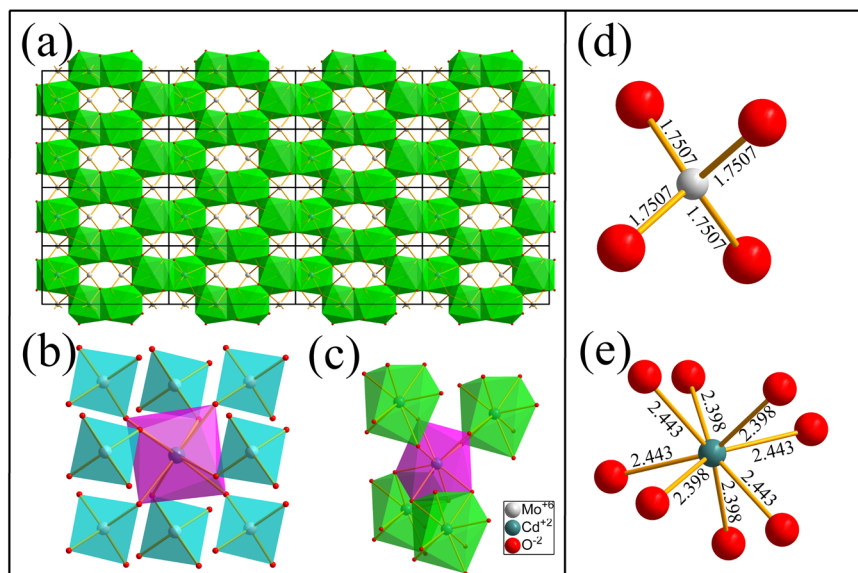


Figure 2. The structure of CdMoO_4 viewed along different directions. The green polyhedron represents Cd^{2+} center and the blue polyhedron represents the Mo^{6+} center.

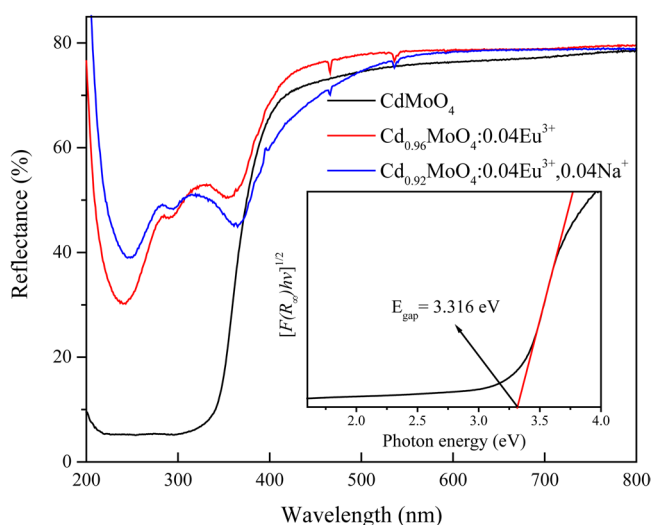


Figure 3. UV-vis diffuse reflection spectra of the as-synthesized CdMoO_4 , $\text{Cd}_{0.96}\text{MoO}_4:0.04\text{Eu}^{3+}$ and $\text{Cd}_{0.92}\text{MoO}_4:0.04\text{Eu}^{3+}, 0.04\text{Na}^+$ phosphors.

reflectance from BaSO_4 as a reference. It is shown in the UV-vis diffuse reflectance spectra in Fig. 3 that these samples have strong absorption band in UV and near UV light region. For CdMoO_4 host, the correlation between the optical band gap E_{gap} and absorption coefficient of semiconductor oxides can be determined by the following equation^{23,24}:

$$F(R_{\infty})hv \propto (hv - E_{\text{gap}})^n \quad (1)$$

$$F(R_{\infty}) = \frac{(1 - R_{\infty})^2}{2R_{\infty}} \quad (2)$$

where ν is the photon energy, R_{∞} is the reflectivity of the sample, h is the Plank constant, and n is determined by the transition type ($n = 1/2, 2, 3/2$ or 3 for allowed direct, allowed indirect, forbidden direct and forbidden indirect electronic transitions, respectively).

According to the calculation results of electronic band structure in Fig. 4, the semi-conducting character of CdMoO_4 has been confirmed to be allowed indirect band gap material, therefore, n is equal to 2.

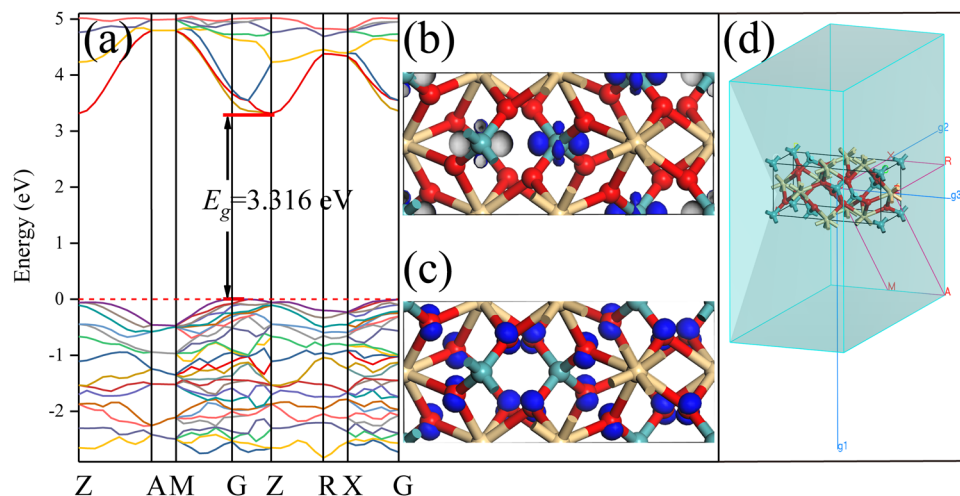


Figure 4. Calculated electronic band structure (a); electron orbitals of excited (b) and ground (c) states of CdMoO₄ near the Fermi energy level (EF); and the Brillouin zone path for band structure calculation (d). The Fermi energy is the zero of the energy scale.

From				To			
Z	0.000	0.000	0.500	A	0.500	0.500	0.500
A	0.500	0.500	0.500	M	0.500	0.500	0.000
M	0.500	0.500	0.000	G	0.000	0.000	0.000
G	0.000	0.000	0.000	Z	0.000	0.000	0.500
Z	0.000	0.000	0.500	R	0.000	0.500	0.500
R	0.000	0.500	0.500	X	0.000	0.500	0.000
X	0.000	0.500	0.000	G	0.000	0.000	0.000
Z	0.000	0.000	0.500	A	0.500	0.500	0.500

Table 1. Brillouin Zone Path.

$$h\nu - E_{gap} \propto [F(R_{\infty})h\nu]^{1/2} \quad (3)$$

As can be seen from the Tauc-plots of CdMoO₄ sample in the inset of Fig. 3, by extrapolating the linear fitted regions to $[F(R_{\infty})h\nu]^{1/2} = 0$, the absorption boundary is 3.316 eV.

For the samples with Eu³⁺ doped, the weak absorption in the visible light region is consistent with the white color of powders for the naked eye. And compared with the commercial red emitting phosphors, CdMoO₄:Eu³⁺ phosphors can effectively avoid the disadvantages such as reabsorption in the visible light region.

In order to figure out the origin of the broad band absorption in the UV-vis diffuse reflection spectra of Fig. 3, the calculation of the electronic structure for CdMoO₄ host was carried out using CASTEP code by density functional theory. The Brillouin zone path for the band structure calculation was shown in Fig. 4(d) and Table 1. The calculated electronic band structure and electron orbitals are given in Fig. 4(a). The lowest energy (2.361 eV) of conduction band (CB) located at Z site, and the valence band (VB) maximum (0.00 eV) is at G site of Brillouin zone, indicating that CdMoO₄ is an indirect band gap compound and the energy band gap is about 2.361 eV. It is well known that the DFT calculations with CASTEP program generally underestimate the band-gap energies of the semiconductor materials due to the limited dimension of the atomic cluster. Therefore, a scissors operator of 0.955 eV was introduced to widen the gap to consistent with the measured optical band gap value (3.316 eV) of CdMoO₄ host.

After first-principle calculation, the electron orbitals were shown in Fig. 4b and c. It is well known that the d orbital splits into d_{xy} , d_{xz} , d_{yz} , d_{z^2} and $d_{x^2-y^2}$ in the tetrahedral crystal field due to the Jahn-Teller effect. The electron orbitals of the Mo atoms in the tetrahedron crystal field are shown in the Fig. 4(b). It can be seen that the excited electrons enter into the d_{z^2} and $d_{x^2-y^2}$ orbitals with low energy. From Fig. 4(b), the states in the conduction band region are dominated by Mo 4d orbitals. Figure 4(c) shows the position of electrons in the valence band region. The shape of electron distribution is two hemispheres which belong to the typical 2p orbitals of O atoms. The diagram of electron orbitals illustrates that the top of VB is mainly composed by 2p orbital of O atom. Therefore, the absorption bands in Fig. 3 are ascribed to electron transitions from oxygen 2p orbital to an empty molybdenum 4d orbital.

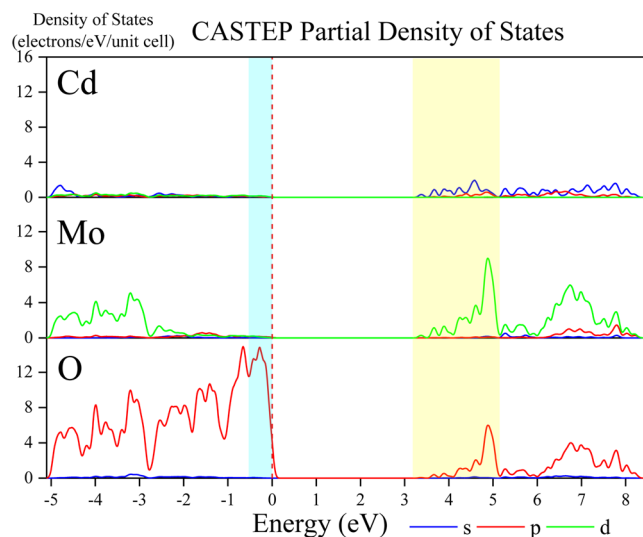


Figure 5. Diagrams of PDOS of Cd/Mo/O for CdMoO₄ host.

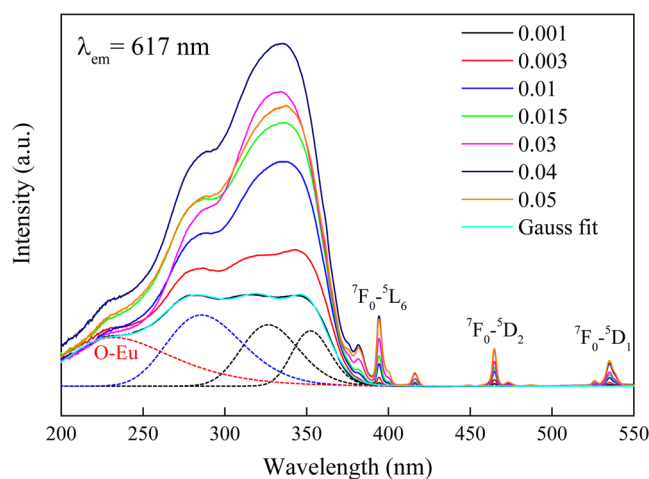


Figure 6. The excitation spectra of Cd_{1-x}MoO₄:xEu³⁺ phosphor monitored at 617 nm emission (⁵D₀ – ⁷F₂) at room temperature.

Taking into account the lower display resolution of the electron orbitals diagram, theoretical calculations on the partial density of states (PDOS) for CdMoO₄ host were carried out and the results are illustrated in Fig. 5. From Fig. 5, the valence bands are dominated by the O 2p states. The integral area of 5s orbitals in the excited states is large enough to be taken into account. It means that the 5s orbitals of Cd atom is an important part of the charge transfer band. The strong hybridization appears between Cd 5s, Mo 4d and O 2p states in the bottom of the conduction bands. The strong absorption bands in Fig. 3 are mainly originated from the charge transfer bands from O 2p to Mo 4d and Cd 5s orbitals.

Photoluminescence properties. A series of Cd_{1-x}MoO₄:xEu³⁺ samples were synthesized to optimize the doping concentration of Eu³⁺ ions. Figure 6 shows the excitation spectra of Cd_{1-x}MoO₄:xEu³⁺ phosphors monitored at ⁵D₀ – ⁷F₂ (617 nm) emission of Eu³⁺ ions. The broad excitation bands ranging from 200 nm to 380 nm are related to the charge transfer transition of O²⁻ → Mo⁶⁺ and O²⁻ → Eu³⁺. According to the reported literature, the sharp peaks at 394 and 465 nm are due to ⁷F₀ – ⁵L₆ and ⁷F₀ – ⁵D₂ transitions of Eu³⁺, respectively. When the doping concentration of Eu³⁺ was less than 4%, the relative intensity of excitation bands increases with the increase of Eu³⁺ concentration. A more interesting thing is that the relative intensity of excitation bands, especially at about 328 nm, enhanced sharply with the increase of Eu³⁺ concentration. However, when the doping concentration of Eu³⁺ was beyond 4%, the intensity of excitation bands decreased with increasing Eu³⁺ concentration.

From Fig. 7, PL and PLE spectra of CdMoO₄, Cd_{0.999}MoO₄:0.001Eu³⁺ and Cd_{0.96}MoO₄:0.04Eu³⁺ phosphors are presented in an immediate contrast. In Fig. 7(a), pure CdMoO₄ sample exhibits a strong green emission band with a maximum at about 504 nm under 337 nm excitation. When monitoring at 504 nm, the PLE spectrum in Fig. 7(a) indicated that the as-synthesized CdMoO₄ phosphor exhibits a broad excitation band in the range of 250–380 nm. Three obvious excitation peaks for CdMoO₄ host were observed at room temperature, which can

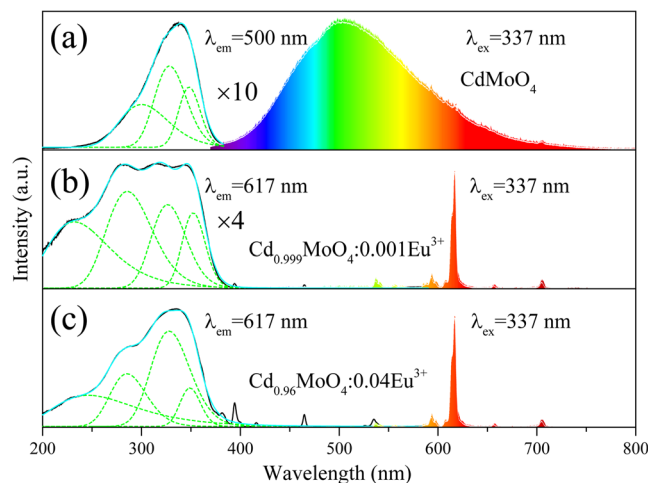


Figure 7. PL and PLE spectra of CdMoO₄ (a); Cd_{0.999}MoO₄:0.001Eu³⁺ (b) and Cd_{0.96}MoO₄:0.04Eu³⁺ (c) phosphors.

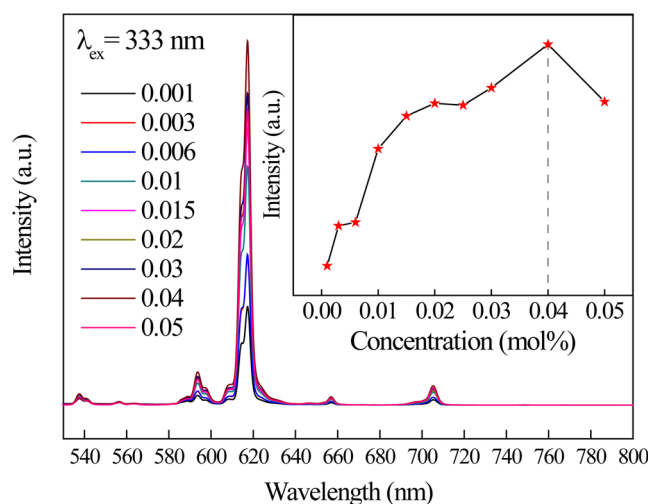


Figure 8. The emission spectra of Cd_{1-x}MoO₄:xEu³⁺ phosphors excited at about 337 nm in room temperature.

be further deconvoluted by assuming a Gaussian type profile into the three excitation peaks at 300 nm, 328 nm and 348 nm, which are attributed to the charge transfer transition of O²⁻ → Mo⁶⁺ and O²⁻ → Cd²⁺ transitions.

As for the Eu³⁺ singly doped CdMoO₄ sample, its PL and PLE spectra are presented in Fig. 7b and c. The PL spectrum under the excitation of 337 nm has a series of sharp line emissions at 594, 617, 657 and 705 nm, due to the ⁵D₀ → ⁷F_J (J = 1, 2, 3 and 4) characteristic transitions of Eu³⁺ ions. The emission peak of CdMoO₄ host could not be observed owing to the energy transfer from CdO₈ and MoO₄ polyhedra to Eu³⁺ ions. In the excitation spectrum of CdMoO₄:Eu³⁺ phosphors monitoring at ⁵D₀ → ⁷F₂ emission of Eu³⁺ ions, the broad absorption band from 200 to 380 nm which was decomposed into four components by Gaussian fitting can be assigned to the combination of the charge transfer (CT) transitions. Compared with the excitation spectra of CdMoO₄ host, the new excitation band at about 246 nm was observed. From Figs 6 and 7b and c it can be seen that the excitation band at about 328 nm enhanced sharply. This is explained by the fact that the CdO₈ and MoO₄ polyhedra in three-dimensional network structure can transfer energy to Eu³⁺ ions.

Figure 8 illustrates the emission spectra of Cd_{1-x}MoO₄:xEu³⁺ (x = 0.001, 0.003, 0.006, 0.01, 0.015, 0.02, 0.03, 0.04, 0.05) phosphors excited at about 337 nm. It can be seen from the picture that the strongest emission peak is at about 617 nm which is caused by the ⁵D₀ → ⁷F₂ electric dipole transition of Eu³⁺ ions. For the Cd_{1-x}MoO₄:xEu³⁺ phosphor, the emission intensities increased with the Eu³⁺ concentration up to 0.04, and then decreases with increasing concentration due to the concentration quenching.

When Eu³⁺ ions are doped into the CdMoO₄ host, with the increase of Eu³⁺ doping concentration, the relative distance between Eu³⁺ ions will be reduced gradually. Their distance (d) can be written as:

$$d = 2 \times \sqrt[3]{\frac{3 \times V}{4 \times \pi \times c \times N}} \quad (4)$$

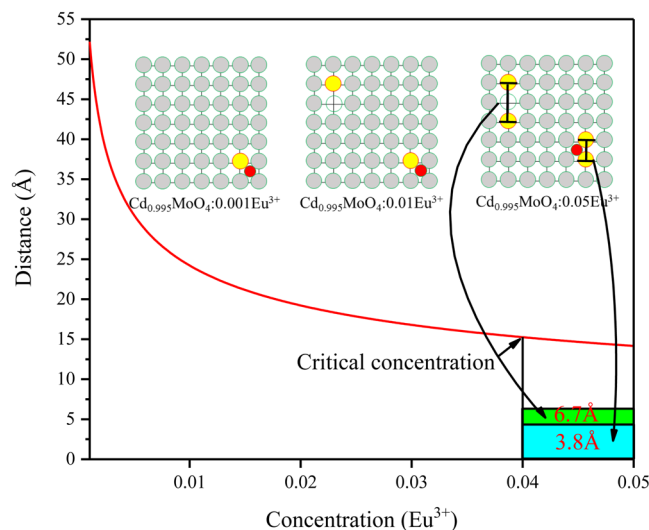
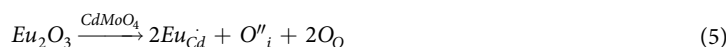


Figure 9. The mechanism of concentration quenching in Eu^{3+} doped $\text{CdMoO}_4:\text{Eu}^{3+}$ phosphor.

where V is the volume of the unit cell, c is the critical concentration of the activator ion, and N is the number of host cations in the unit cell. For the CdMoO_4 host, by taking the values of $N = 4$ ($N = Z \times 1$, Z is the number of formula per unit cell) and $V = 297.64 \text{ \AA}^3$, the relative distance between Eu^{3+} ions (d) varies with the doping concentration (c) as shown in Fig. 9.

When the doping concentration of Eu^{3+} is low, Eu^{3+} ions are dispersed in the CdMoO_4 host. The relative distance decreases sharply with the increase of doping concentration. When the concentration of doped Eu^{3+} is more than the critical concentration, it will no longer follow the Equation (4) due to the defect reaction in Equations (5 and 6). As a result, some of Eu^{3+} ions will enter into the adjacent lattice sites and share a point defect (V''_{Cd} or O''_i) to achieve charge balance. The defect equations are as follows:



Combined with the crystal structure, we believe that the position of point defects are as shown in Fig. 9. In $\text{CdMoO}_4:\text{Eu}^{3+}$ phosphor, Eu^{3+} is an isolated emission center which has been reported that the typical critical distance is about 5 Å. That is to say, the exchange interaction becomes effective when the $\text{Eu}^{3+} - \text{Eu}^{3+}$ distance is shorter than 5 Å. When the concentration of Eu^{3+} is low, the interaction of $\text{Eu}^{3+} - \text{Eu}^{3+}$ can be almost neglected because of the long distance between Eu^{3+} ions. However, the relative distance is only about 3.8 Å when two Eu^{3+} ions occupy adjacent Cd sites. This indicates that the mechanism of exchange interaction plays an important role in energy transfer between the adjacent Eu^{3+} ions in $\text{CdMoO}_4:\text{Eu}^{3+}$ phosphor. And the point defect of O''_i is also detrimental to the luminescence of Eu^{3+} ions. This is the reason why concentration quenching occurred.

The charge imbalance caused by trivalent Eu^{3+} ions occupying divalent Cd^{2+} sites in the CdMoO_4 host affects the intensity of PL spectra. We believe that the distance between Eu^{3+} ions can be regulated by charge compensation²⁵. Therefore, the variation of PL intensity with different charge compensator doping concentrations is displayed in Fig. 10. As can be observed in this picture, the effect of charge compensators, Li^+ , Na^+ , K^+ ions and Cd^{2+} vacancy, on red emission of Eu^{3+} is enhanced markedly. The photoluminescence intensity of $\text{Cd}_{0.96-y}\text{MoO}_4:0.04\text{Eu}^{3+}, y\text{Li}^+$, $\text{Cd}_{0.96-y}\text{MoO}_4:0.04\text{Eu}^{3+}, y\text{Na}^+$ and $\text{Cd}_{0.96-y}\text{MoO}_4:0.04\text{Eu}^{3+}$ phosphors reached the maximum when the charge is balanced. This indicates that the charge imbalance affects the photoluminescence properties of Eu^{3+} ions in CdMoO_4 host. The maximum PL intensity is reached when the concentration of K^+ ions in $\text{Cd}_{0.96-y}\text{MoO}_4:0.04\text{Eu}^{3+}, y\text{K}^+$ is 0.02. This is caused by the presence of lattice distortion that affects the photoluminescence properties. The lattice expansion corresponds to the larger ionic radius of K^+ (1.51 Å) than that of Cd^{2+} (1.10 Å).

From above we can see that both Li^+ , Na^+ , K^+ and Cd^{2+} vacancies can significantly enhance the fluorescence intensity of $\text{CdMoO}_4:\text{Eu}^{3+}$ phosphors. In order to compare the photoluminescence enhancement of different charge compensators, the excitation spectra of $\text{Cd}_{0.96-y}\text{MoO}_4:0.04\text{Eu}^{3+}, y\text{M}$ ($\text{M} = \text{Li}^+, \text{Na}^+, \text{K}^+$ ions and Cd^{2+} vacancy) phosphors were shown in Fig. 11. Selected concentrations of charge compensator are the optimum doping concentration of Li^+ , Na^+ , K^+ ions and Cd^{2+} vacancies. As can be seen from Fig. 11, the photoluminescence intensity is increased by two times when Na^+ ions were introduced as charge compensator. So why a small amount of charge compensator can greatly improve the fluorescence intensity?

The Mechanism of Charge Compensation. Figure 12 shows the radius and relative position of doping ions in charge compensated $\text{CdMoO}_4:\text{Eu}^{3+}$ system. It can be seen that the ionic radius of Eu^{3+} and Cd^{2+} ions are

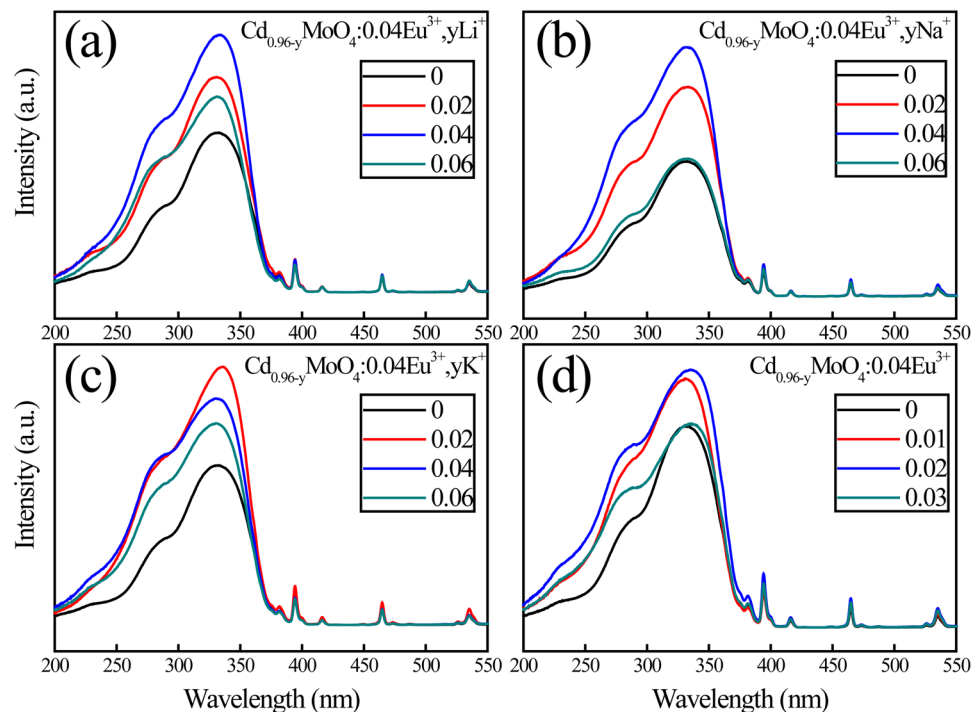


Figure 10. Excitation spectra of $\text{Cd}_{0.96-y}\text{MoO}_4:0.04\text{Eu}^{3+}, y\text{M}$ ($\text{M} = \text{Li}^+, \text{Na}^+, \text{K}^+$ ions) and $\text{Cd}_{0.96-y}\text{MoO}_4:0.04\text{Eu}^{3+}$ phosphors monitoring at 617 nm in room temperature.

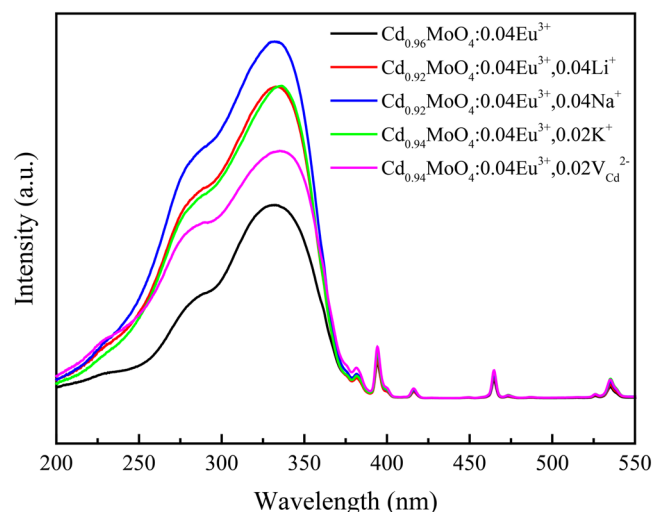


Figure 11. Excitation spectra of $\text{Cd}_{0.96-y}\text{MoO}_4:0.04\text{Eu}^{3+}, y\text{M}$ ($\text{M} = \text{Li}^+, \text{Na}^+, \text{K}^+$ ions and Cd^{2+} vacancy) phosphors.

approximately equal. Therefore, Eu^{3+} can successfully occupy the Cd^{2+} lattice. On the basis of this theoretical development, Li^+ , Na^+ , K^+ ions and Cd^{2+} vacancies were introduced as a charge compensators because a large number of lattice defects appeared with the introduction of Eu^{3+} ions.

The possible relative position of doping ions in CdMoO_4 host and photoluminescence enhancement mechanism is shown in Fig. 13. The diagram explains how the introduced Li^+ , Na^+ , K^+ ions and Cd^{2+} vacancy break the interaction of Eu^{3+} ions. The point defect reaction of the cation sublattice was written as Equations (5 and 6). In particular, a certain amount of interstitial occupation of O atoms (O''_i) is introduced into the lattice due to the charge imbalance by $\text{Eu}^{3+}/\text{Cd}^{2+}$. This leads to the increase of cell parameters and the decrease of luminescence intensity of Eu^{3+} ions. Due to the smaller ion radius of Li^+ ions, some of interstitial occupation of doping Li^+ ions (Li'_i) and O^{2-} ions (O''_i) appear in the $\text{Cd}_{0.92}\text{MoO}_4:0.04\text{Eu}^{3+}, 0.04\text{Li}^+$ sample. The point defect reaction of the cation sublattice was written as Equation (7). Therefore, the interstitial occupation of Li^+ ions increased the cell parameters. When the concentration of Li^+ ions increased more than 0.04, A large amount of (Li'_i) and (O''_i) will

Ion Type	Ionic Radius (Å) Eight coordination
Cd^{2+}	1.10
Eu^{3+}	1.066
Li^+	0.92
Na^+	1.18
K^+	1.51
Mo^{6+}	0.41

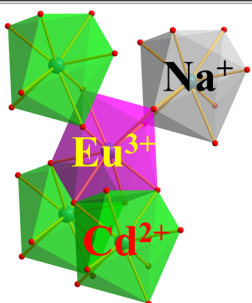


Figure 12. Ionic radius and relative positions of doping ions.

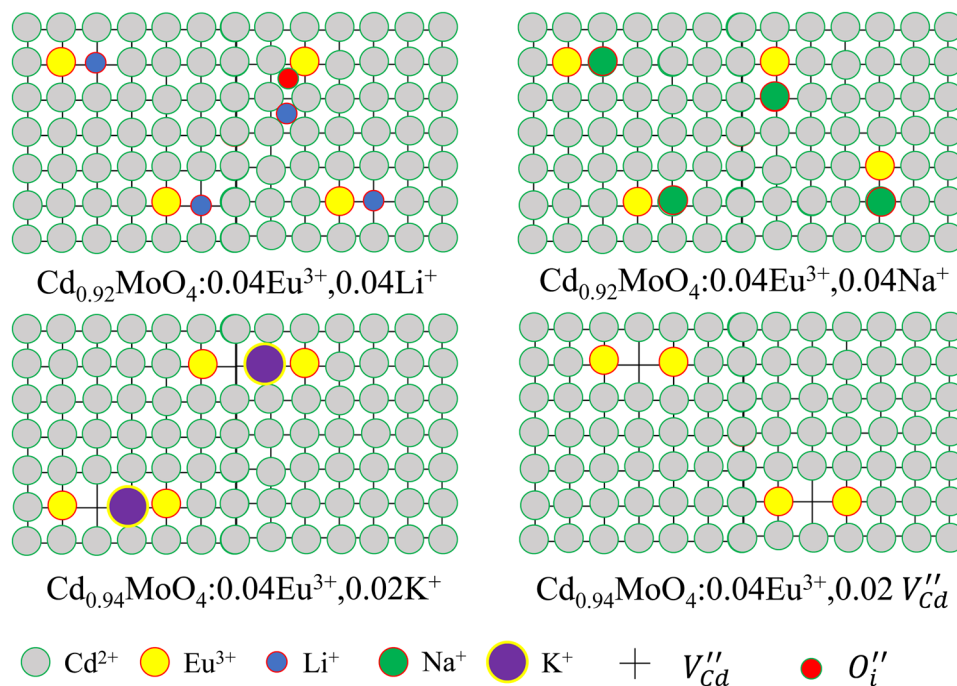
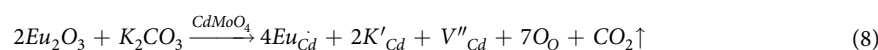
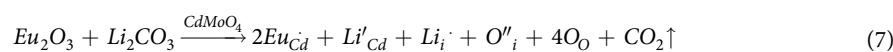


Figure 13. The schematic diagram of luminescence enhancement mechanisms with different charge compensators.

appear to reduce the photoluminescence intensity of Eu^{3+} ions. The point defect reaction of the K^+ cation sublattice may be written as Equation (8). The large ionic radius of K^+ ions resulted in the highest lattice distortion in the sample. As can be seen in Fig. 13, the lattice shrinkage induced by the point defect of Eu_{Cd} and V''_{Cd} were compensated by the great lattice expansion of the K'_{Cd} defect. The appropriate concentration of K^+ ions gives the best optical performance. Because the appearance of $\text{Eu}_{\text{Cd}} - V''_{\text{Cd}}$ pair can stabilize the luminescent environment of the $\text{Eu}_{\text{Cd}} - \text{K}'_{\text{Cd}}$ pair. The point defects equation with Cd^{2+} vacancy is Equations (9 and 10). Therefore, the introduction of V''_{Cd} reduced the point defect of O''_i and thus increased the photoluminescence intensity.

The ionic radius of Na^+ ions is most approaching to Cd^{2+} , and the introduction of Na^+ ions can produce a negative charge. The introduction of Na^+ ions can also reduce the structural distortion well because of the suitable ionic radius. This results in the concentration decrease of O''_i and thus decrease the cell parameters. Therefore, as a charge compensator, Na^+ ions have an ideal ion radius and charge states. The point defect reaction of the Na^+ cation sublattice may be written as Equation (11). Eu^{3+} and Na^+ ions will occupy the adjacent Cd^{2+} ion lattice sites in order to achieve charge balance and reduce the lattice distortion. Therefore, the introduction of Na^+ ions can compensate the effect of the charge imbalance well, which can significantly enhance the luminescence intensity of Eu^{3+} ions.



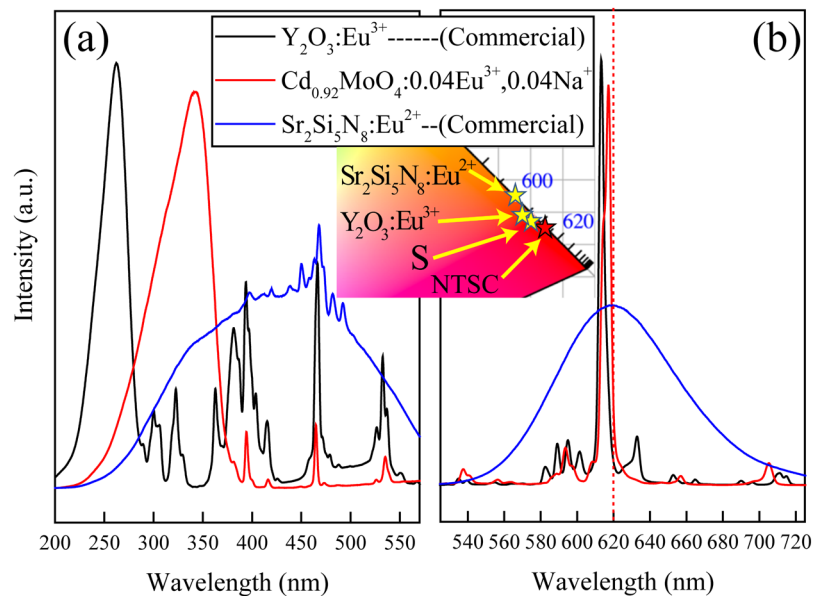
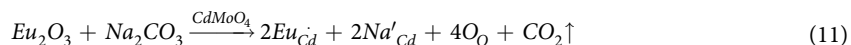
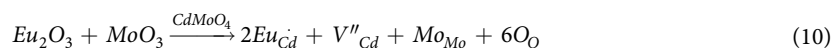


Figure 14. The PLE (a), PL (b) spectra and chromaticity coordinates in Commission Internationale de l'Éclairage (CIE) 1931 color spaces (insert) of prepared $\text{Cd}_{0.92}\text{MoO}_4:0.04\text{Eu}^{3+}, 0.04\text{Na}^+$ phosphor compared with those of commercial red-emitting phosphor ($\text{Y}_2\text{O}_3:\text{Eu}^{3+}$ and $\text{Sr}_2\text{Si}_5\text{N}_8:\text{Eu}^{2+}$).



With the purpose of application for white-light LEDs with near-UV based chips as excitation sources, photoluminescence properties of $\text{Cd}_{0.92}\text{MoO}_4:0.04\text{Eu}^{3+}, 0.04\text{Na}^+$ and commercial red emission phosphors are compared. Figure 14a and b shows the intuitive compared PL and PLE spectra of $\text{Cd}_{0.92}\text{MoO}_4:0.04\text{Eu}^{3+}, 0.04\text{Na}^+$ and commercial $\text{Y}_2\text{O}_3:\text{Eu}^{3+}$ and $\text{Sr}_2\text{Si}_5\text{N}_8:\text{Eu}^{2+}$ red emitting phosphors under the same measurement conditions. According to the compared spectra, the intensity of the broad excitation band at about 345 nm and sharp emission peak at about 617 nm in $\text{Cd}_{0.92}\text{MoO}_4:0.04\text{Eu}^{3+}, 0.04\text{Na}^+$ phosphors were high enough to be comparable to commercial red-emitting phosphors. The ${}^5\text{D}_0 - {}^7\text{F}_2$ emission intensity of $\text{Cd}_{0.92}\text{MoO}_4:0.04\text{Eu}^{3+}, 0.04\text{Na}^+$ is about 94% of $\text{Y}_2\text{O}_3:\text{Eu}^{3+}$ commercial phosphor. The CIE chromaticity diagram of prepared $\text{Cd}_{0.92}\text{MoO}_4:0.04\text{Eu}^{3+}, 0.04\text{Na}^+$ and commercial red emitting phosphors was shown in the insert of Fig. 14. It can be seen that the optimal $\text{Cd}_{0.92}\text{MoO}_4:0.04\text{Eu}^{3+}, 0.04\text{Na}^+$ approaches the National Television System Committee (NTSC) ideal red color ($x=0.67, y=0.33$) and it is much closer to the red region on the CIE chromaticity diagram than commercial $\text{Sr}_2\text{Si}_5\text{N}_8:\text{Eu}^{2+}$ and $\text{Y}_2\text{O}_3:\text{Eu}^{3+}$ phosphors. Thus, as-prepared $\text{Cd}_{0.92}\text{MoO}_4:0.04\text{Eu}^{3+}, 0.04\text{Na}^+$ phosphor is promising red-emitting phosphor for near-UV- LEDs.

Conclusion

In summary, a series of Eu^{3+} and alkali metal ions co-doped CdMoO_4 phosphors were prepared by the solid-state reaction method in air atmosphere. In CdMoO_4 crystal structure, CdO_8 and MoO_4 polyhedra were connected with each other by coplanar to form a 3D network. Eu^{3+} ions occupied Cd^{2+} sites will be excited with the energy collected by 3D network structure. In addition, eight adjacent MoO_4 polyhedra can also effectively transfer energy to the Eu^{3+} ion. However, the interaction between Eu^{3+} ions is further amplified in the 3D network structure. The introduced $\text{Li}^+, \text{Na}^+, \text{K}^+$ ions and Cd^{2+} vacancy which can avoid O''_i will separate the couple of Eu^{3+} ions and break the interaction between them. Since the suitable ionic radius and valence states, the introduction of Na^+ can break the energetic interaction of Eu^{3+} ions through the 3D network structure. This is because the introduction of Na^+ ions can decrease the lattice distortion and avoid the appearance of O''_i point defect. This mechanism provides a model how to use charge compensator to break the energetic interaction between Eu^{3+} ions which expected to be used to design efficient luminescent materials.

Experiment

Materials and Synthesis. A series of Eu^{3+} doped CdMoO_4 phosphors were synthesized by a traditional high temperature solid state reaction in air atmosphere. Stoichiometric amounts of CdO (99.9%), Eu_2O_3 (99.99%) and MoO_3 (99%) were mixed homogeneously in an agate mortar. The mixtures were put into an alumina crucible and calcined in the muffle furnace at 800 °C for 3 hours in air atmosphere, and then the white powder phosphor

was obtained. In some cases, appropriate amounts of Li_2CO_3 (99.9%), Na_2CO_3 (99.9%) and K_2CO_3 (99.9%) were added as charge compensators. In order to reduce the amount of Cd in the sample and increase the concentration of Cd vacancy, the stoichiometry of CdO is intentionally reduced. All samples were ground into a powder in an agate mortar and pestle for further analysis.

Experimental methods. The phase purity was verified by the powder X-ray diffraction (XRD) measurement performed on a Bruker D8 Advance X-ray diffractometer (Cu $\text{K}\alpha_1$ radiation, $\lambda = 0.15406$ nm) and high-resolution X-ray diffraction was recorded over an angular (2θ) range of $5\text{--}130^\circ$ with radiation at a 0.02° (2θ)/s scanning step. Structural refinements of X-ray diffractograms were performed by the GSAS2 program. UV-Vis diffuse reflectance spectra (DRS) were collected using a V-670 (JASCO) UV-Vis spectrophotometer. The photoluminescence excitation (PLE) and emission (PL) spectra were recorded with a Hitachi F-4600 spectrophotometer equipped with a 150 W xenon lamp as an excitation source at room temperature. DFT calculations on the CdMoO_4 host was carried out by using the CASTEP code²¹. All the measurements were performed at room temperature.

Details of calculation. The CASTEP program was employed to determine the Band structure and Orbital population by density functional theory^{26–28}. The Vanderbilt ultrasoft pseudopotential with a cutoff energy of 380 eV was used to ensure the precision of the results. Brillouin zone integration was represented using the K-point sampling scheme of $3 \times 3 \times 1$ Monkhorst–Pack scheme²⁹. At first, the Broyden, Fletcher, Goldfarb, Shanon (BFGS) method was used to achieve the geometry optimization. Atomic positions and lattice parameters were optimized simultaneously during the geometry optimization. The convergence tolerance for geometry optimization was selected with the differences in total energy (5.0×10^{-6} eV/atom), the maximal ionic Hellmann–Feynman force (1.0×10^{-2} eV/Å), the stress tensor (2.0×10^{-2} GPa), and the maximal displacement (5.0×10^{-4} Å). The calculations were conducted within the generalized gradient approximations (GGA), using the exchange and correlation functional. The convergence criterion for the self-consistent field (SCF) was set to 5.0×10^{-7} eV/atom in whole processes.

References

- Feldmann, C., Thomas, J., Cees, R. R. & Peter, J. S. Inorganic luminescent materials: 100 years of research and application. *Adv Funct Mater* **13**, 511–516, <https://doi.org/10.1002/adfm.200301005> (2003).
- Ye, S., Xiao, F., Pan, Y., Ma, Y. & Zhang, Q. Phosphors in phosphor-converted white light-emitting diodes: Recent advances in materials, techniques and properties. *Mat Sci Eng R* **71**, 1–34 (2010).
- Shimizu, Y., Sakano, K., Noguchi, Y. & Moriguchi, T. Light emitting device with blue light LED and phosphor components. US patent US6614179 B1 (2003).
- Titkov, I. E. *et al.* Superior color rendering with a phosphor-converted blue-cyan monolithic light-emitting diode. *Laser Photonics Rev* **10**, 1031–1038, <https://doi.org/10.1002/lpor.201600196> (2016).
- Nakamura, S. & Fasol, G. *The blue laser diode-GaN based light emitters and lasers*. 1 edn 216–221 (Springer-Verlag Berlin Heidelberg, 1997).
- Steigerwald, D. A. *et al.* Illumination with solid state lighting technology. *IEEE J Sel Top Quant* **8**, 310–320, <https://doi.org/10.1109/2944.999186> (2002).
- Sheu, J. K. *et al.* White-light emission from near UV InGaN-GaN LED chip precoated with blue/green/red phosphors. *IEEE Photonic Tech L* **15**, 18–20, <https://doi.org/10.1109/LPT.2002.805852> (2003).
- Xia, Z., Zhou, J. & Mao, Z. Near UV-pumped green-emitting $\text{Na}_3(\text{Y}, \text{Sc})\text{Si}_3\text{O}_9:\text{Eu}^{2+}$ phosphor for white-emitting diodes. *J Mater Chem C* **1**, 5917–5924, <https://doi.org/10.1039/C3TC30897A> (2013).
- Zheng, J. *et al.* An efficient blue-emitting $\text{Sr}_3(\text{PO}_4)_3:\text{Cl}:\text{Eu}^{2+}$ phosphor for application in near-UV white light-emitting diodes. *J Mater Chem C* **3**, 11219–11227, <https://doi.org/10.1039/C5TC02482J> (2015).
- Dai, P. *et al.* $\text{Sr}_3\text{Ce}(\text{PO}_4)_3:\text{Eu}^{2+}$: a broadband yellow-emitting phosphor for near ultraviolet-pumped white light-emitting devices. *J Mater Chem C* **4**, 1170–1177, <https://doi.org/10.1039/C5TC02582F> (2016).
- Deng, J. *et al.* Eu^{3+} -Doped Phosphor-in-Glass: A Route toward Tunable Multicolor Materials for Near-UV High-Power Warm-White LEDs. *Adv Opt Mater* **5**, 1600910, <https://doi.org/10.1002/adom.201600910> (2017).
- Zhou, H., Wang, Q. & Jin, Y. Temperature dependence of energy transfer in tunable white light-emitting phosphor $\text{BaY}_2\text{Si}_3\text{O}_{10}:\text{Bi}^{3+}, \text{Eu}^{3+}$ for near UV LEDs. *J Mater Chem C* **3**, 11151–11162, <https://doi.org/10.1039/C5TC02514A> (2015).
- Zhang, H., Niu, C.-G., Wen, X.-J., Wang, Y. & Zeng, G.-M. Enhanced visible light photocatalytic activity of CdMoO_4 microspheres modified with AgI nanoparticles. *Catal Commun* **86**, 124–128 (2016).
- Madhusudan, P., Zhang, J., Cheng, B. & Yu, J. Fabrication of $\text{CdMoO}_4@ \text{CdS}$ core-shell hollow superstructures as high performance visible-light driven photocatalysts. *Phys Chem Chem Phys* **17**, 15339–15347, <https://doi.org/10.1039/C5CP01598G> (2015).
- Ran, W. *et al.* A super energy transfer process based S-shaped cluster in ZnMoO_4 phosphors: theoretical and experimental investigation. *J Mater Chem C*, 8344–8350, <https://doi.org/10.1039/C5TC01583A> (2015).
- Wang, W. S., Zhen, L., Xu, C. Y., Shao, W. Z. & Chen, Z. L. Eu^{3+} -doped CdMoO_4 red phosphor synthesized through an aqueous solution route at room temperature. *J Alloys Compd* **529**, 17–20 (2012).
- Lin, J., Zeng, Z. & Wang, Q. $\text{CdMoO}_4:\text{Eu}^{3+}$ micro-sized luminescent particles synthesis and photo-catalytic performance. *Inorg Chim Acta* **408**, 59–63 (2013).
- Guzik, M., Tomaszewicz, E., Guyot, Y., Legendziewicz, J. & Boulon, G. Eu^{3+} luminescence from different sites in a scheelite-type cadmium molybdate red phosphor with vacancies. *J Mater Chem C* **3**, 8582–8594, <https://doi.org/10.1039/C5TC01109D> (2015).
- Liu, X., Lv, L., Huang, S., Su, Y. & Wang, X. Microwave-Assisted Synthesis and Luminescence Properties of $\text{Cd}_{1-x}\text{Eu}_x\text{MoO}_4$ Red Phosphor. *J Nanosci Nanotechnol* **14**, 3618–3622, <https://doi.org/10.1166/jnn.2014.7992> (2014).
- Guzik, M., Tomaszewicz, E., Guyot, Y., Legendziewicz, J. & Boulon, G. Structural and spectroscopic characterizations of new $\text{Cd}_{1-x}\text{Nd}_x\text{MoO}_4$ scheelite-type molybdates with vacancies as potential optical materials. *J Mater Chem C* **3**, 4057–4069, <https://doi.org/10.1039/C4TC02963A> (2015).
- Segall, M. D. *et al.* First-principles simulation: ideas, illustrations and the CASTEP code. *J Phys: Condens Mat* **14**, 2717–2744 (2002).
- Toby, B. H. & Von Dreele, R. B. GSAS-II: the genesis of a modern open-source all purpose crystallography software package. *J Appl Crystallogr* **46**, 544–549, <https://doi.org/10.1107/S0021889813003531> (2013).
- Morales, A. E., Mora, E. S. & Pal, U. Use of diffuse reflectance spectroscopy for optical characterization of un-suspended nanostructures. *Revista Mexicana de Fisica S* **53**, 18–22 (2007).
- Wood, D. L. & Tauc, J. Weak Absorption Tails in Amorphous Semiconductors. *Phys Rev B* **5**, 3144–3151 (1972).

25. Ran, W., Wang, L., Tan, L., Qu, D. & Shi, J. Remote Control Effect of Li^+ , Na^+ , K^+ Ions on the Super Energy Transfer Process in $\text{ZnMoO}_4:\text{Eu}^{3+}$, Bi^{3+} Phosphors. *Sci Rep* **6**, 27657, <https://doi.org/10.1039/C5TC01583A> (2016).
26. Hohenberg, P. & Kohn, W. Inhomogeneous electron gas. *Phys Rev* **136**, B864–B871 (1964).
27. Kohn, W. & Sham, L. J. Self-consistent equations including exchange and correlation effects. *Phys Rev* **140**, A1133–A1138 (1965).
28. Payne, M. C., Teter, M. P., Allan, D. C., Arias, T. & Joannopoulos, J. Iterative minimization techniques for ab initio total-energy calculations: molecular dynamics and conjugate gradients. *Rev Mod Phys* **64**, 1045–1097 (1992).
29. Monkhorst, H. J. & Pack, J. D. Special points for Brillouin-zone integrations. *Phys Rev B* **13**, 5188–5192 (1976).

Acknowledgements

This research was supported by the Basic Science Research Program through the National Research Foundation of Korea (NRF) funded by the Ministry of Science, ICT and Future Planning (No. 2018R1A2B6005179). The $\text{CdMoO}_4:\text{Eu}^{3+}$, M (M = Li^+ , Na^+ , K^+ ions and Cd^{2+} vacancy) phosphors were supplied by the Functional Phosphor Bank at Pukyong National University.

Author Contributions

Weiguang Ran performed the sample preparation, designed the whole research and completed the writing of the manuscript. Hyeon Mi Noh and Sung Heum Park performed all the experimental tests. Byung Kee Moon analyzed the XRD data. Jinsheng Shi revised the articles and proposed many good suggestions. The whole work was carried out under the guidance of Jung Hyun Jeong and Jung Hwan Kim. All the authors discussed the results and commented on the manuscript.

Additional Information

Competing Interests: The authors declare no competing interests.

Publisher's note: Springer Nature remains neutral with regard to jurisdictional claims in published maps and institutional affiliations.



Open Access This article is licensed under a Creative Commons Attribution 4.0 International License, which permits use, sharing, adaptation, distribution and reproduction in any medium or format, as long as you give appropriate credit to the original author(s) and the source, provide a link to the Creative Commons license, and indicate if changes were made. The images or other third party material in this article are included in the article's Creative Commons license, unless indicated otherwise in a credit line to the material. If material is not included in the article's Creative Commons license and your intended use is not permitted by statutory regulation or exceeds the permitted use, you will need to obtain permission directly from the copyright holder. To view a copy of this license, visit <http://creativecommons.org/licenses/by/4.0/>.

© The Author(s) 2018